average volume of a microdomain. The inverse of equation (*A*5) becomes

$$\varepsilon_1^2(\mathbf{q}) = v_0 \left(\frac{V}{N_d}\right) \sum_l \frac{\alpha_l'}{C_l^{(11)}} \exp(2\pi i \mathbf{q} \cdot \mathbf{R}_l). \qquad (A6)$$

Up to equation (*A*5), $\varepsilon_1^2(\mathbf{q})$ is defined as a function concentrated only around $\mathbf{q}=0$. In equation (*A*6), $\varepsilon_1^2(\mathbf{q})$ is given as a periodic function in the fundamental lattice, as the α_l' parameters are defined only at the direct lattice points. If $\varepsilon_1^2(\mathbf{q})$ is sufficiently concentrated in the vicinity of a reciprocal-lattice point, the distribution just around $\mathbf{q}=0$ may be regarded as $\varepsilon_1^2(\mathbf{q})$ given in equation (*A*5). Thus, the mean shape function is obtained from the experimental intensity data using equations (*A*3) and (*A*6). At this stage, there is still uncertainty in the value of N_d in (*A*6). The following consideration will help determine it.

The function $E_1(\mathbf{r})$ may be regarded as a sort of order parameter according to the definition in equation (6). If each site within a microdomain is occupied by the correct atom for the ordered structure, $E_1(\mathbf{r})$ becomes unity, as was given in equation (6), and if the degree of order decreases with increasing distance from the centre of the microdomain, it changes from 1 to 0 with increasing distance $|\mathbf{r}|$. According to this consideration, the following equation holds:

$$E_1(\mathbf{r}=0) = \int \varepsilon_1(\mathbf{q}) d\mathbf{q} = 1. \qquad (A7)$$

Here, $|\varepsilon_1(\mathbf{q})|$ can be obtained directly from the experimental data using equation (*A*6), but $\varepsilon_1(\mathbf{q})$ cannot. In the non-correlation model considered here, however, $\varepsilon_1^2(\mathbf{q})$ may be approximated by a smooth function such as a Cauchy, Gaussian, exponential function, *etc.*, and then $\varepsilon_1(\mathbf{q})$ may be a smooth positive function. In most practical cases, $\varepsilon_1(\mathbf{q})$ in equation (*A*7) may be safely replaced by $|\varepsilon_1(\mathbf{q})|$. Using $|\varepsilon_1(\mathbf{q})|$ obtained from equations (*A*6) and (*A*7), N_d is evaluated.

It is inferred from equation (*A*5*a*) that $E_1^2(\mathbf{r})$ represents the distribution of size and shape of microdomains.

References

BATTERMAN, B. (1956). Ph. D. Thesis, Massachusetts Institute of Technology, Cambridge, Mass.

COWLEY, J. M. (1950). *J. Appl. Phys.* **21**, 24–30.

GEHLEN, P. C. & COHEN, J. B. (1965). *Phys. Rev.* **139**, A844–A855.

GREENHOLZ, M. & KIDRON, A. (1970). *Acta Cryst.* A**26**, 311–314.

GUINIER, A. (1963). *X-Ray Diffraction*, Translated by P. LORRIAN. San Francisco: W. H. Freeman.

HASHIMOTO, S. & OGAWA, S. (1970). *J. Phys. Soc. Japan*, **29**, 710–721.

MOSS, S. C. (1966). *Local Atomic Arrangements Studied by X-Ray Diffraction*, Edited by J. B. COHEN & J. E. HILLIARD, pp. 95–122. New York: Gordon & Breach.

MOSS, S. C. (1969). *Phys. Rev. Lett.* **22**, 1108–1111.

OSHIMA, K. & WATANABE, D. (1973). *Acta Cryst.* A**29**, 520–526.

SATO, K., WATANABE, D. & OGAWA, S. (1962). *J. Phys. Soc. Japan*, **17**, 1647–1651.

WATANABE, D. (1959). *J. Phys. Soc. Japan*, **14**, 436–443.

WILSON, A. J. C. (1962). *X-Ray Optics*. New York: John Wiley.

YAMAGUCHI, S., WATANABE, D. & OGAWA, S. (1962). *J. Phys. Soc. Japan*, **17**, 1030–1041.

Acta Cryst. (1974). A**30**, 798

Some Neutron Diffraction Experiments on Curved Silicon Crystals

BY A. BOEUF AND F. RUSTICHELLI

Institut Laue Langevin, Grenoble, France and Physics Division, CCR Euratom

(*Received* 10 *April* 1974; *accepted* 16 *June* 1974)

The diffraction properties of curved silicon crystals, with curvature radii between ∞ and 25 m obtained by microscopic techniques, were investigated by means of a neutron diffractometer. The ratio of neutron reflectivity between plane and curved silicon crystals was measured as a function of the neutron wavelength using different reflecting planes in both Bragg and Laue cases in symmetrical and asymmetrical conditions. The experimental results were interpreted with the results of theoretical investigations on the dynamical theory of diffraction applied to the curved-crystal case. The implications of this work on neutron monochromator design are briefly discussed.

1. Introduction

The problem of neutron diffraction by curved crystals has been treated theoretically (Klar & Rustichelli, 1973) by an extension of the dynamical theory for X-ray diffraction (Taupin, 1964*a*, *b*). The aim of this work was to give an experimental contribution in the same field of the physics of neutron diffraction by curved crystals. The ratio of neutron reflectivities between perfect plane crystals and curved crystals with the same

characteristics has been measured at different wavelengths using varying reflecting planes. As a consequence, either the incident Bragg angle or the reflexion asymmetry was changed during the experiment. Most of the measurements were done in the Bragg reflexion condition and few of them in the Laue reflexion condition. The experimental data were compared with theoretical values expected from the dynamical diffraction theory for ideally curved crystals mentioned above. Knowledge of the neutron diffraction by curved crystals finds an interesting application in the design of new types of neutron monochromators as, for instance, crystals curved by microscopic techniques (Rustichelli, 1968), by temperature gradient (Alefeld, 1969), or by other techniques (Egert & Dachs, 1970), crystals grown with a gradient in the lattice spacing (Rustichelli, 1972), and furthermore in the design of composite neutron monochromator systems (Boeuf & Rustichelli, 1973).

2. Experimental technique

(*a*) *The silicon crystals*

The perfect silicon crystals were crystalline disks, 0·5 and 1 mm thick respectively, and 40 mm in diameter. The curved silicon crystals were obtained from perfect crystalline disks of the same size, chemically bent to different curvatures (see Table 1). The curvature was obtained by high-temperature reaction of silicon with a gaseous mixture of N_2,SiH_4 and NH_3 which produces a Si_3N_4 film on the silicon. Owing to the fact that the Si_3N_4 film and the silicon have different thermal expansion coefficients, a curvature is obtained when the crystal is cooled down. This curvature depends on the thickness of the original silicon disk and on the thickness of the Si_3N_4 film. Disks of different curvatures have been produced by varying the two parameters. The treatment was done at the L.E.T.I. Laboratories (Grenoble). More details on the procedure used and on the control carried out during the fabrication can be found in Antonini, Corchia, Nicotera & Rustichelli (1972).

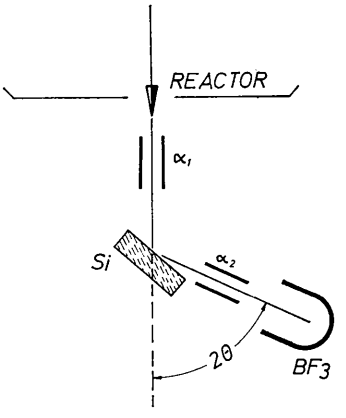

Fig. 1. Sketch of the geometrical configuration of the experimental set-up.

Table 1. *Characteristics of the silicon crystals used*

Crystal identification	Thickness (mm)	Thickness of Si_3N_4 layer (Å)	Radius of curvature (m)
A_0	0·5	0	∞
B_0	0·5	5000	35
C_0	0·5	10000	20
A_1	1	0	∞
B_1	1	5000	90
C_1	1	10000	55

In the silicon crystals used, the surface was cut parallel to the (111) reflecting plane. The diffraction from the (111) reflecting plane at different Bragg angles was first investigated in Bragg symmetrical conditions. Then the diffraction from the (551) reflecting plane, which forms an angle $\varphi=27°$ with the face of the crystal, was studied at different θ angles using Bragg asymmetrical conditions. Finally, diffraction from the (115) reflecting plane, which forms an angle $\varphi=39°$ with the face of the crystal, was investigated at different θ angles in Bragg and Laue asymmetrical conditions.

(*b*) *Neutron diffraction measurements*

The neutron diffraction experiments were carried out at the T2 tangential channel of the Mélusine reactor of CEN Grenoble. A well collimated polychromatic beam of about 10 mm height and 1 mm width, having a horizontal divergence of about 16′, was impinging on the tested silicon crystals as shown in Fig. 1. The diffracted neutron intensity was detected by a BF3 counter positioned at a certain 2θ Bragg angle depending on the chosen wavelength. An optimization of the position of the tested crystal was made and all the diffracted intensity was recorded with an almost infinite divergence between crystal and counter. In this way, for each 2θ angle, *i.e.*, for a given neutron wavelength and for a given reflecting plane, the ratio of the intensity diffracted by the curved crystal to the intensity diffracted by the non-curved crystal of the same dimension was recorded. By this technique, only the effect of the different curvatures is analysed at a given neutron wavelength for a given reflecting plane and for a given diffraction asymmetry.

3. Neutron diffraction results

(*a*) *Directly recorded data*

The results of the different measurements are presented in Figs. 2–6. I_c is the neutron intensity measured with the curved silicon crystal and I_p is the neutron intensity measured with a non-curved silicon crystal of the same size under the same conditions: the measured ratio is then given by $A_p^c=I_c/I_p$ and is reported in the figures as a function of the wavelength of the diffracted neutrons. In Fig. 2 the results obtained in symmetrical Bragg conditions for the (111) reflecting plane and for a 0·5 mm thick crystal are reported. Fig. 3 gives the ratio A_p^c obtained in the same geometri-

cal conditions but for a silicon crystal 1 mm thick. From this curve it can be seen that at a wavelength of about 1 Å the neutron intensity reflected by the curved silicon crystal is approximately six times greater than the intensity reflected by the non-curved silicon crystal. Figs. 4 and 5 concern measurements made under asymmetrical Bragg conditions using as reflecting plane the (551) silicon plane for the 0·5 mm thick and the 1 mm thick crystals respectively. Finally, Fig. 6 reports the neutron intensity ratio A_p^c obtained by diffraction from the silicon (115) plane in asymmetrical Laue conditions and in the asymmetrical Bragg condition for a 1 mm thick crystal. One can see that the behaviour of the curved crystals is quite similar in the two geometrical conditions when the incident beam direction approaches very closely the surface of the crystal, *i.e.* when λ approaches the limiting value of 1·3 Å which separates the Bragg and Laue conditions.

(*b*) *Derivation of absolute reflecting powers for the curved crystals*

The results presented in Figs. 2 to 6 can be utilized to calculate the integral reflecting power as a function of the neutron wavelength for curved crystals. If one chooses the neutron wavelength as independent variable, the integral reflecting power is defined as follows:

$$R_H^\lambda = \int_{-\infty}^{+\infty} \frac{P_H}{P_0} \cdot \mathrm{d}\lambda \qquad (1)$$

where P_H is the neutron diffracted power and P_0 is the incident neutron power. The measured quantity A_p^c, which is the ratio of the diffracted neutron intensity of a curved crystal to that of a non-curved crystal, also represents the ratio of the reflecting power of the curved crystal to that of the non-curved crystal

$$A_p^c = \frac{I_c}{I_p} = \frac{R_c^\lambda}{R_p^\lambda \cdot \xi} \qquad (2)$$

where R_c^λ is the integral reflecting power of the curved crystal, R_p^λ is the integral reflecting power of the non-curved crystal and ξ is a correction factor taking into account the fact that the non-curved crystals (A_0 and A_1) used are not quite perfect. The degree of imperfection of such crystals has been measured previously, and ξ is deduced from the measurements made at $\lambda = 1{\cdot}2$ Å and reported in Table 1 of Antonini *et al.* (1972), supposing to a first approximation that ξ remains constant in the range of wavelength investigated. The value of R_p^λ, integral reflecting power of a perfect crystal, can be calculated from the following formula (Zachariasen, 1967)

$$R_p^\lambda = \frac{4d^3 F_H}{V_c} \cdot \frac{\sin\theta}{\sqrt{\frac{\gamma_0}{\gamma_H}}} \qquad (3)$$

in the Bragg condition, and

$$R_p^\lambda(\text{Laue}) = \frac{1}{2} R_p^\lambda(\text{Bragg}), \qquad (4)$$

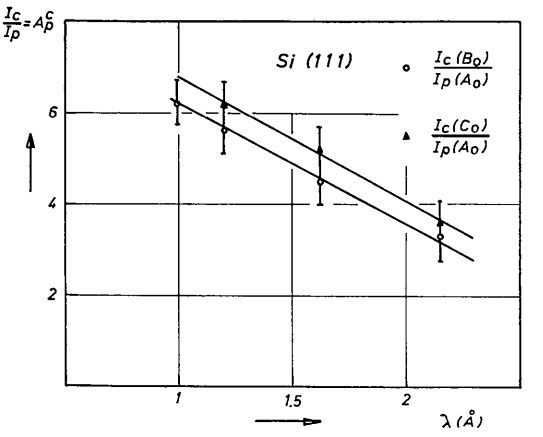

Fig. 2. The ratio between the neutron intensity diffracted by the curved and the non-curved crystals as a function of the wavelength for the (111) plane and the 0·5 mm thick crystal.

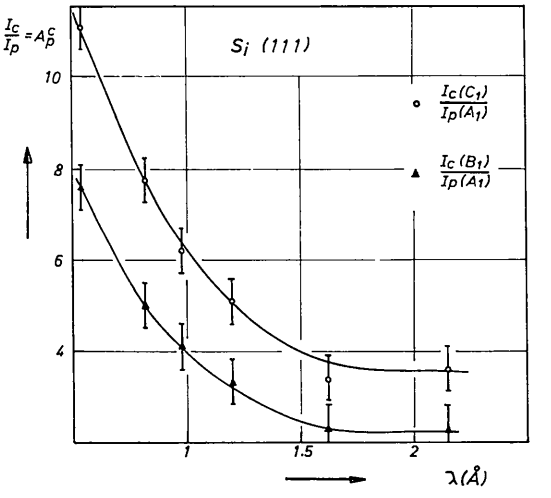

Fig. 3. The ratio between the neutron intensity diffracted by the curved and the non-curved crystals as a function of the wavelength for the (111) plane and the 1 mm thick crystal.

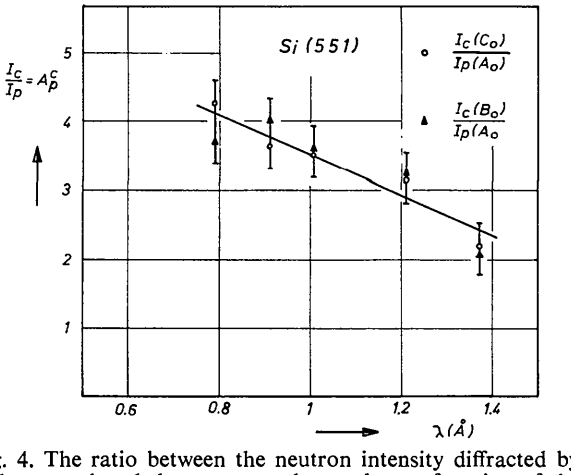

Fig. 4. The ratio between the neutron intensity diffracted by the curved and the non-curved crystals as a function of the wavelength for the (551) plane and the 0·5 mm thick crystal.

where d is the lattice spacing of the plane considered, F_H is the structure factor, V_c is the volume of the elementary cell, θ is the Bragg angle, γ_0 and γ_H are the direction cosines of the incident and diffracted waves respectively. In Table 2, the values of R_c^λ deduced from experimental results using equations (2)–(4) are reported for the different wavelengths and for the different reflecting planes investigated.

4. Interpretation of experimental results

(*a*) *Theoretical considerations on crystal curvature*

In order to interpret the data, further elaboration is needed based on the following considerations. From elementary geometrical observations, it can be seen that the curvature radius ϱ, the thickness Δt and the angular disorientation along the incident beam (between the two faces of the crystal) $\Delta\theta$, are related by the equation

$$\Delta\theta = \frac{\Delta t}{\varrho} \cdot \cot\alpha\,, \tag{5}$$

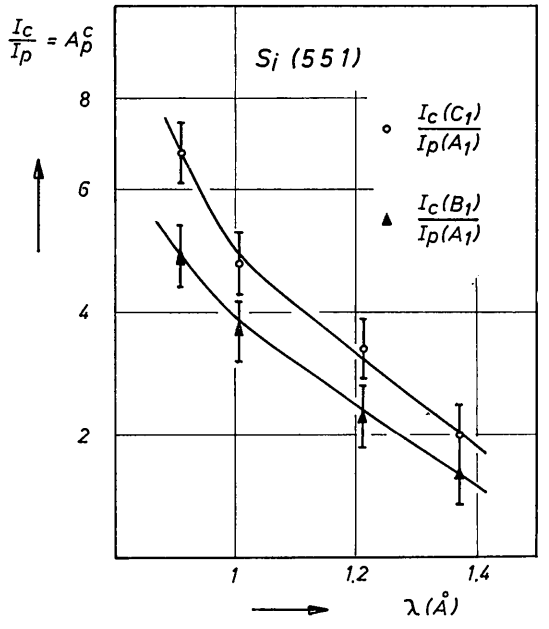

Fig. 5. The ratio between the neutron intensity diffracted by the curved and the non-curved crystals as a function of the wavelength for the (551) plane and the 1 mm thick crystal.

where α is the angle between the incident beam and the crystal surface. In Klar & Rustichelli (1973) a quantity c, which is related to the curvature of the crystal, was defined as

$$c = \frac{\mathrm{d}y}{\mathrm{d}A} \tag{6}$$

where y is the deviation from the Bragg condition expressed in units equal to the halfwidth of the Darwin curve, and A is the total thickness of the crystal expressed in units equal to one half of the extinction length. Taking into account the relation between Δt and $\Delta\theta$ through the variables A and y from (5) and (6), one obtains for the general asymmetrical case, in analogy with the symetrical case treated in Appendix A of Klar & Rustichelli (1973):

$$\varrho = \frac{1}{c} \cdot \frac{\mathrm{d}t}{\mathrm{d}A} \cdot \frac{\mathrm{d}y}{\mathrm{d}\theta} \cdot \cot\alpha\,. \tag{7}$$

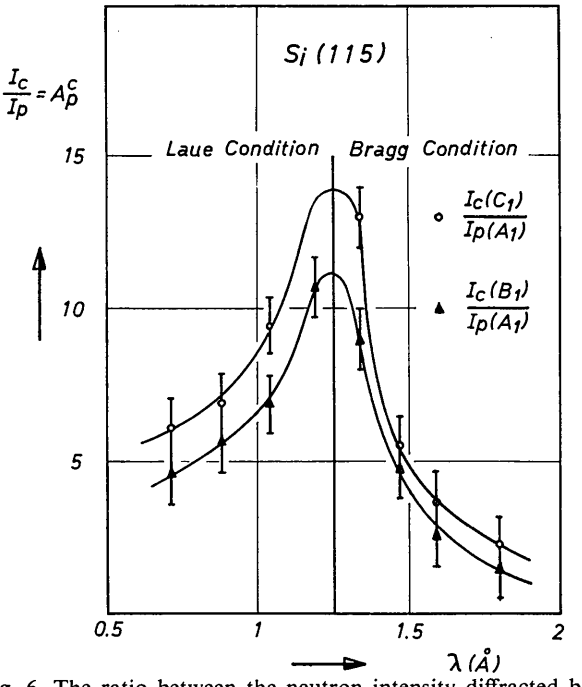

Fig. 6. The ratio between the neutron intensity diffracted by the curved and the non-curved crystals as a function of the wavelength for the (115) plane and the 1 mm thick crystal. For $\lambda < 1{\cdot}3$ Å one obtains the Laue condition and for $\lambda > 1{\cdot}3$ Å one obtains the Bragg condition.

Table 2. *The reflectivity R_c^λ as a function of λ*

	Si(111) $R_c^\lambda \times 10^{12}$					Si(551) $R_c^\lambda \times 10^{12}$					Si(115) $R_c^\lambda \times 10^{12}$		
λ (Å)	B_0	C_0	B_1	C_1	λ (Å)	B_0	C_0	B_1	C_1	λ (Å)	B_1	C_1
0·54	3·53	–	4·65	6·82	0·79	0·463	0·549	1·07	1·215	0·71	0·107	0·141
0·82	4·96	–	4·61	7·16	0·91	0·353	0·324	0·552	0·743	0·88	0·133	0·164
0·98	5·32	4·81	4·49	6·82	1·02	0·282	0·273	0·373	0·484	1·04	0·148	0·202
1·2	5·88	6·50	4·46	6·86	1·21	0·243	0·235	0·217	0·320	1·19	0·160	–
1·62	6·41	7·39	4·19	6·21	1·37	0·154	0·163	0·126	0·183	1·34	0·244	0·350
2·15	6·21	6·77	5·52	8·69						1·47	0·267	0·305
										1·59	0·209	0·289

By using the following relation (Klar & Rustichelli, 1973) between the different variables,

$$\frac{dt}{dA} = t_{ext} \tag{8}$$

$$\frac{dy}{d\theta} = \frac{1}{\Delta\theta(\text{Darwin})}, \tag{9}$$

equation (7) becomes

$$\varrho = \frac{1}{c} \cdot \frac{t_{ext}}{\Delta\theta(\text{Darwin})} \cdot \cot\alpha \,. \tag{10}$$

The curvature corresponding to a value $c=1$ presents particular features. In fact, in this case it can be seen from equation (6) that there is an angular variation in the inclination of lattice plane $\Delta y=2$, *i.e.*, equal to the width of the Darwin curve for a depth variation inside the crystal of $A=2$, *i.e.*, for an extinction length. This can also be seen by comparing equations (10) and (6). In the case of c equal to one, a model can be imagined according to which the curved crystal is decomposed in several layers, each having a thickness equal to the extinction length and disoriented relative to each other by an angle equal to the width of the Darwin curve. It is expected from this model that each layer gives rise (in the diffraction pattern) to a contribution equal to a Darwin curve and adjacent layers give rise to adjacent Darwin curves, as explained in Klar & Rustichelli (1973). This case will be analysed better below. The condition $c=1$ corresponds to the optimum condition when the curved crystal is used as neutron monochromator. In fact, in this case one obtains the maximum diffracted intensity for a given energy resolution. The curvature radius corresponding to $c=1$ will then be called ϱ_{opt}. If $c\neq 1$, one obtains from equation (10)

$$\varrho = \frac{1}{c}\varrho_{opt} \,. \tag{11}$$

If $c<1$, the height of the resulting Darwin curves will be one, as before, but the total width giving the integral reflectivity will be less than the total width corresponding to $c=1$ (Klar & Rustichelli, 1973). On the other hand, the total width of the diffraction pattern becomes larger than in the case $c=1$ but one has no more total reflexion because, at a fixed lattice spacing value, there are not enough lattice planes to give complete primary extinction (Klar & Rustichelli, 1973). Then the optimal curvature radius and the c values can be calculated from the following expressions, which are valid in the more general asymmetric case for the extinction length and the Darwin curve width,

$$t_{ext} = \frac{2V_c[\sin\alpha \,.\, \sin\beta]^{1/2}}{\lambda \,.\, F_H} \tag{12}$$

$$\Delta\theta(\text{Darwin}) = \frac{4F_H d^2}{V_c \pi}\left[\frac{\sin\beta}{\sin\alpha}\right]^{1/2} \,.\, \text{tg}\,\theta \tag{13}$$

where α and β are the angles between the surface of the crystal and the incident beam and the reflected beam respectively, and θ the Bragg angle. From these two equations one obtains

$$\varrho = \frac{1}{c} \cdot \frac{\pi}{2} \frac{V_c^2}{F_H^2 d^2} \frac{1}{\lambda} \cos\alpha \,.\, \cot\theta \tag{14}$$

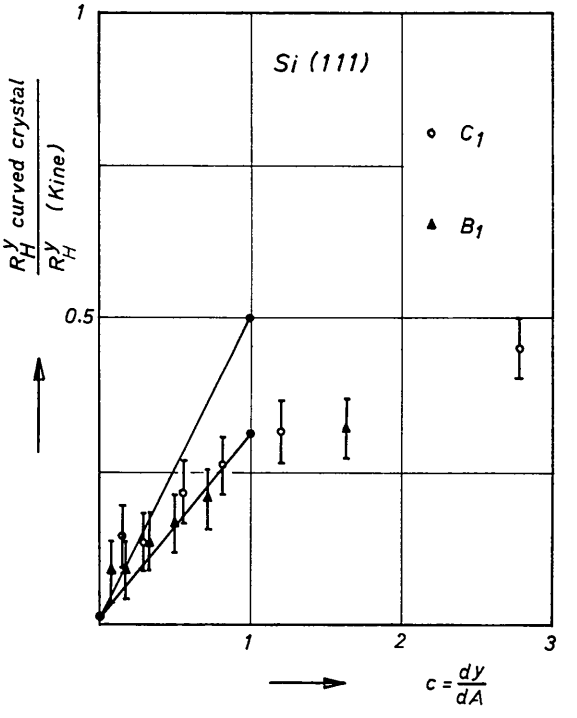

Fig. 7. The integrated reflecting power normalized by the kinematical reflecting power as a function of the crystal curvature for the (111) plane and the 1 mm thick crystals.

Table 3. *The quantity c as a function of the neutron wavelength*

Si(11)		c			Si(551)		c			Si(115)	c	
λ (Å)	B_0	C_0	B_1	C_1	λ (Å)	B_0	C_0	B_1	C_1	λ (Å)	B_1	C_1
0·54	4·22	7·39	1·64	2·69	0·79	13·4	23·5	5·22	8·54	0·71	1·94	3·18
0·82	1·86	3·26	0·72	1·19	0·91	9·6	16·7	3·72	6·09	0·88	1·05	1·72
0·98	1·29	2·25	0·50	0·82	1·02	6·98	12·3	2·73	4·46	1·04	0·59	0·97
1·2	0·86	1·5	0·33	0·54	1·21	3·90	6·85	1·52	2·49	1·19	0·33	0·54
1·62	0·45	0·79	0·17	0·29	1·37	2·17	3·8	0·84	1·38	1·34	0·18	0·29
2·15	0·24	0·42	0·09	0·15						1·47	0·08	0·13
										1·59	0·02	0·03

which in the case of $c=1$ gives ϱ_{opt}. The optimal curvature radius depends for a given crystal on the reflecting plane, the neutron wavelength and the asymmetry of the diffraction. In the present case, the curvature radii of the crystals are constant but owing to the fact that ϱ_{opt} depends on the wavelength, c will also depend on the wavelength, according to equation (11). From the values of the real curvature of the crystals and from equation (14), one obtains the value of c as a function of the wavelength (see Table 3). Table 3 permits us to see immediately for a given diffraction condition whether the crystal considered is curved too much or too little as compared to the optimal condition at which it should be used as neutron monochromator. For a given reflecting plane, it is possible in this way to associate a value of c with each experimental point, and therefore to draw a curve giving R_H^y as a function of c, where R_H^y represents the integral reflecting power in y units (Zachariasen, 1967).

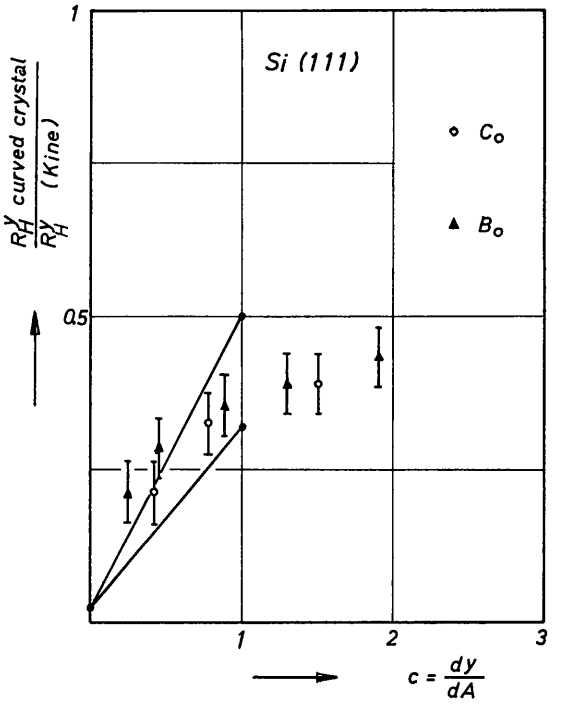

Fig. 8. The integrated reflecting power normalized by the kinematical reflecting power as a function of the crystal curvature for the (111) plane and the 0·5 mm thick crystals.

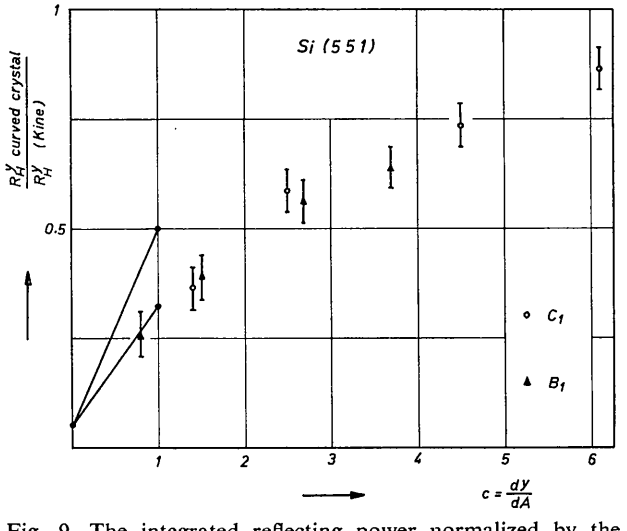

Fig. 9. The integrated reflecting power normalized by the kinematical reflecting power as a function of the crystal curvature for the (551) plane and the 1 mm thick crystals.

It has been shown (Taupin, 1964*a*, *b*) that for a fixed wavelength, when a crystal is progressively curved, the reflecting power R_H^y starts from the dynamical values for $c=0$ and increases asymptotically until it reaches the kinematical reflecting power R_H^y(kine). On the other hand, in our case the value of the curvature radius ϱ is fixed but the neutron wavelength changes. However, one expects that in this case also R_H^y will reach the asymptotic value. But in our asymmetrical reflexion condition, the kinematical reflecting power depends on the neutron wavelength, *i.e.*, on the quantity c. In order to eliminate this wavelength dependence, the values of R_H^y deduced from the experimental measurements have been normalized with the kinematical reflecting power R_H^y(kine) calculated for each c value by the following formula:

$$R_H^y(\text{kine}) = \frac{2\pi d F_H t}{V_c} \cdot \frac{\sin\theta}{\sqrt{(\sin\alpha \,.\, \sin\beta)}} \qquad (15)$$

where t is the real thickness of the crystal. The transformation of the initial data in the form of R_H^y/R_H^y(kine) as a function of c, for a given reflecting plane, allows an easy physical interpretation.

(b) Discussion

One expects that the ratio R_H^y/R_H^y(kine) tends toward one when c tends to infinity. On the other hand, for $c=0$, the above ratio is clearly given by R_H^y(dyn)/R_H^y(kine) by supposing the crystal to be perfect. In addition to the cases $c=0$ and $c=\infty$, the case $c=1$ is particularly interesting and needs a detailed discussion. Before treating this latter case, it is worthwhile to remember that it was observed (Antonini *et al.*, 1972) that

$$R_H^y(\text{kine}) = R_H^y(\text{dyn}) \,.\, A \,. \qquad (16)$$

For a crystal having a thickness $A=2$, equal to the extinction length, R_H^y(kine) is then equal to twice R_H^y(dyn).

From the previously mentioned model of the curved crystal in the case $c=1$ according to which the crystal itself was decomposed into n perfect crystal layers, where n is the ratio of the thickness of the crystal to the extinction length, one expects that

$$R_H^y = n \,.\, R_H^y(\text{dyn}) \,. \qquad (17)$$

The condition proceeds immediately from the observation that for $c=1$, the layers give rise to adjacent

Darwin curves and that R_H^y(dyn) is just the integral reflecting power of a Darwin curve in which the tails are included. From this model and from equation (16), it is expected that for $c=1$, the value R_H^y is equal to one half of the kinematical value, which corresponds indeed to $c=\infty$. This is valid when the wavelength is fixed and the curvature of the crystal is changed or when, as in our case, the curvature is fixed but the wavelength is changed. Therefore for $c=1$, we expect in each case that the ratio R_H^y/R_H^y(kine)$=0{\cdot}5$. Actually 0·5 represents a maximum value for this ratio, as will be explained below. Indeed, in the model developed by Klar & Rustichelli (1973) and adapted to the crystal with a gradient of lattice parameter (Rustichelli, 1972) for $c=1$, the crystal is decomposed into n elementary layers each one reflecting a Darwin curve which is supposed to be a rectangle. In such a model, one neglects, therefore, the tails of the Darwin curves, which is equivalent to replacing in equation (2) the value of R_H^y(dyn), which is given by

$$R_H^y(\text{dyn})=\int_{-\infty}^{+\infty}\frac{P_H}{P_0}(y)\,.\,\mathrm{d}y \qquad (19)$$

with

$$R_H^y(\text{dyn})_{\text{RECT.}}=\int_{-1}^{+1}\frac{P_H}{P_0}(y)\,.\,\mathrm{d}y\,. \qquad (20)$$

The ratio between integrals (20) and (19) is equal to $2/\pi$ (Zachariasen, 1967). With this last approximation for $c=1$, it is expected that $R_H^y/R_H^y(\text{kine})=1/\pi$ for all the reflecting planes considered. In conclusion, for the asymptotic value $c=\infty$ and for $c=1$, the theoretical values of the ratio R_H^y/R_H^y(kine) are expected to be independent of the neutron wavelength used, of the reflecting plane considered and of the thickness of the crystal, as long as this is bigger than one extinction length. Taking into account the previous considerations for $c=1$, the ratio R_H^y/R_H^y(kine) is expected to lie between an upper value of 0·5 and a lower value of $1/\pi$. However, for $c=0$ and therefore for the values of c included between 0 and 1, the ratio R_H^y/R_H^y(kine) depends on the reflecting plane considered and for a given reflecting plane on the crystal thickness (Zachariasen, 1967). Fig. 7 shows the ratio R_H^y/R_H^y(kine) as a function of c for the 1 mm thick crystal with the (111) plane as reflecting plane in symmetrical Bragg conditions. Fig. 8 shows the ratio R_H^y/R_H^y(kine) (c) in the same diffraction condition for the 0·5 mm thick crystals. Figs. 9 and 10 give the ratio R_H^y/R_H^y(kine) (c) for the (551) reflecting plane in asymmetrical Bragg conditions for 1 mm thick and the 0·5 mm thick crystals respectively. In Fig. 11, the same quantity is reported for the 1 mm thick crystals and for the (115) reflecting plane in asymmetrical Bragg conditions. Fig. 12 shows the ratio R_H^y/R_H^y(kine) (c) for the 1 mm thick crystals and for the (115) reflecting plane in asymmetrical Laue conditions. In each of these figures, two straight lines are drawn which join the theoretical value of R_H^y/R_H^y(kine) expected at $c=0$ and given by equation (3) and the upper and lower values of $\frac{1}{2}$ and $1/\pi$ respectively, expected at $c=1$ for the same function.

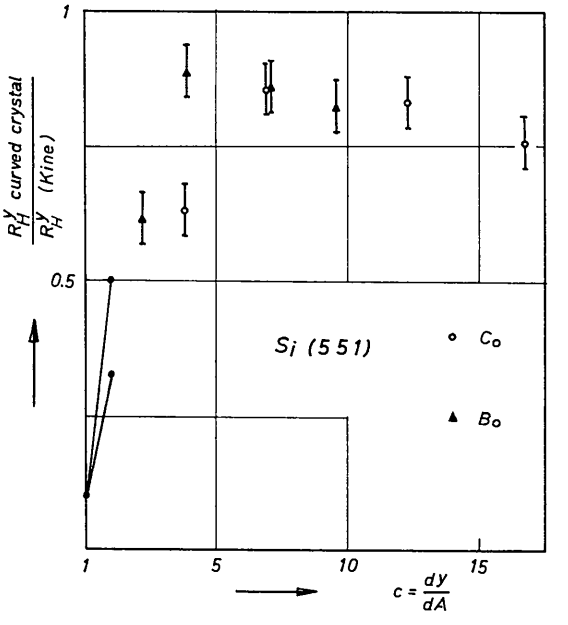

Fig. 10. The integrated reflecting power normalized by the kinematical reflecting power as a function of the crystal curvature for the (551) plane and the 0·5 mm thick crystals.

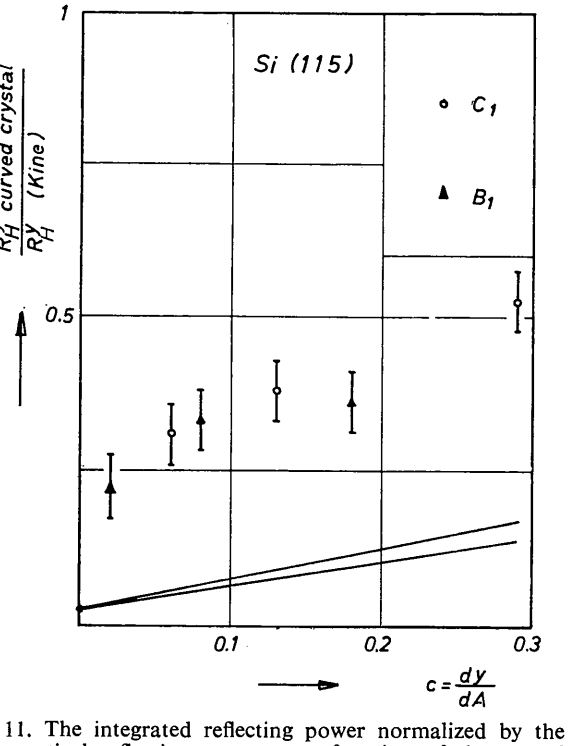

Fig. 11. The integrated reflecting power normalized by the kinematical reflecting power as a function of the crystal curvature for the (115) plane and the 1 mm thick crystal in the Bragg condition.

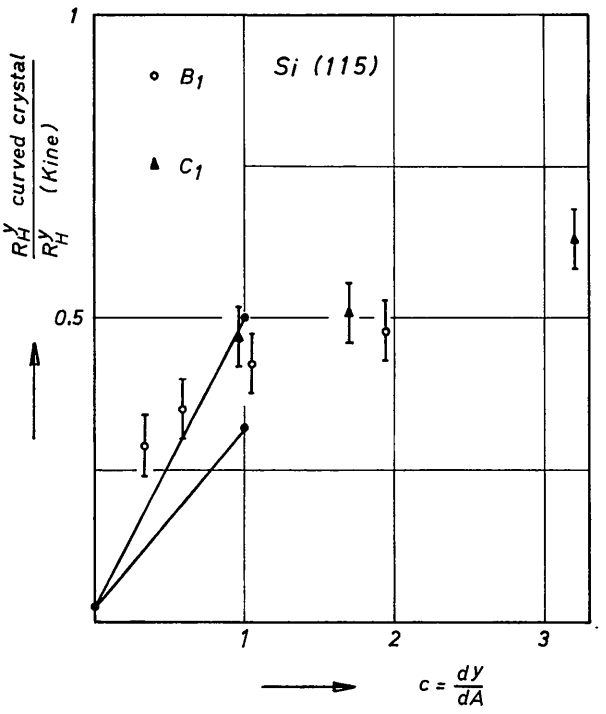

Fig. 12. The integrated reflecting power normalized by the kinematical reflecting power as a function of the crystal curvature for the (115) plane and the 1 mm thick crystal in the Laue condition.

From the observation of the different figures, it appears that in spite of a lack of complete agreement between theoretical and experimental values, similar behaviour is observed for all the diffracting planes utilized, as expected on the basis of the theoretical considerations. In particular, with the exception of Fig. 11 a satisfactory quantitative agreement exists in the range $0<c<1$, which is the most interesting for application in the field of neutron monochromatization. On the other hand, the data of Fig. 11 correspond to a very small curvature for which the intrinsic imperfection of our particular crystals become more important than those corresponding to the curvature itself, as was seen in Antonini *et al.* (1972). Concerning the transmission Laue case, it can be seen that the layer model introduced for $c=1$ is still valid, which explains the similar behaviour observed for Laue and Bragg cases.

Conclusion

The ratio of neutron reflectivity between plane and curved silicon crystals was measured as a function of the neutron wavelength using different reflecting planes on crystals of different thicknesses and curvatures in both Bragg and Laue conditions. This work has been related to the theoretical results which were obtained recently by applying the dynamical theory of neutron diffraction to ideally curved crystals. Owing to the fact that in the experiments the neutron wavelength was changed, the interpretation of the experimental results was not straightforward and needed an elaboration of the rough data on the basis of several physical considerations. As a result of this elaboration, all the data were arranged in a quite general form, which allows a satisfactory explanation of the results. Moreover, the measurements performed are of particular interest in the design of neutron monochromators and composite focusing systems.

References

ALEFELD, B. (1969). *Z. Phys.* **228**, 454–464.
ANTONINI, M., CORCHIA, M., NICOTERA, E. & RUSTICHELLI, F. (1972). *Nucl. Instrum. Meth.* **104**, 147–152.
BOEUF, A. & RUSTICHELLI, F. (1973). *Nucl. Instrum. Meth.* **107**, 429–435.
EGERT, G. & DACHS, H. (1970). *J. Appl. Cryst.* **3**, 214–220.
KLAR, B. & RUSTICHELLI, F. (1973). *Nuovo Cim.* **13B**, 249–271.
RUSTICHELLI, F. (1968). SIF No. 62–41.
RUSTICHELLI, F. (1972). IAEA-SM155/F-2, 697–711.
TAUPIN, D. (1964*a*). Thèse, Université de Paris.
TAUPIN, D. (1964*b*). *Bull. Soc. Fr. Minér. Cryst.* **87**, 469–511.
ZACHARIASEN, W. H. (1967). *Theory of X-Ray Diffraction*, pp. 111–129. Dover: New York.